

GT2011-46, ' %

## EFFECTS OF TARGET SIZE ON FOREIGN OBJECT DAMAGE IN GAS-TURBINE GRADE SILICON NITRIDES BY STEEL BALL PROJECTILES

**Sung R. Choi\***

Naval Air Systems Command, Patuxent River, MD 20670

**Zsolt Rác**

FACC AG, Ried im Innkreis, Austria

### ABSTRACT

Foreign object damage (FOD) phenomena of two gas-turbine grade silicon nitrides (AS800 and SN282) were assessed at ambient temperature applying impact velocities from 20 to 300 m/s using 1.59-mm diameter hardened steel ball projectiles. Targets in a flexural configuration with two different sizes (thicknesses) of 1 and 2 mm were ballistic-impacted under a fully supported condition. The severity of impact damage, as well as the degree of post-impact strength degradation, increased with increasing impact velocity, increased with decreasing target size, and was greater in SN282 than in AS800 silicon nitride. The critical impact velocity where targets fractured catastrophically decreased with decreasing target size and was lower in SN282 than in AS800. Overall, FOD by steel projectiles was significantly less than that by silicon-nitride ceramic counterparts, due to much decreased Hertzian contact stresses. A correlation of backside cracking velocity versus target size was made based on a simplified elastic foundation analysis.

[*Keywords:* foreign object damage (FOD); impact damage; impact test; silicon nitrides; ceramics; ballistic impact; target size effect]

### INTRODUCTION

Ceramics, because of their brittle nature, are prone to localized surface damage and/or cracking when subjected to impact by foreign objects. It is also obvious that ceramic components may fail catastrophically or structurally even by relatively soft particles when the kinetic energy of the impacting objects exceeds certain limits. Phenomena of

particle impact have been frequently encountered in aeroengines where combustion products, metallic particles, sand, thermal barrier coatings (TBCs) loosened from a combustor, or small foreign objects ingested cause damage to related components, resulting in structural or functional problems. Hence, foreign object damage (FOD) associated with particle impact needs to be considered when ceramic materials, either monolithic ceramics or ceramic matrix composites (CMCs), are designed for aeroengine applications such as combustor liners and stationary or rotating airfoils. A significant amount of work on impact of brittle materials by different projectiles or plates has been done experimentally and analytically in the past for a variety of applications including gas turbine engines [1-18].

Series of FOD work on two gas-turbine grade silicon nitrides (AS800 and SN282) have been performed using flexure bars or disks [19-22]. Targets in a rigid support were ballistic-impacted by hardened chrome-steel (SAE 52100) ball projectiles with a diameter of 1.59 mm using an impact velocity range of 220 to 440 m/s. AS800 silicon nitride exhibited a greater FOD resistance than SN282, attributed to greater fracture toughness of AS800. Assessments of FOD in AS800 silicon nitride were also made using four different projectile materials of 1.59-mm-diameter hardened steel, annealed (at 350 and 700°C) steel, silicon nitride, and brass balls [23-26]. The hardness of the projectile materials was a key parameter affecting the most amount of impact damage. The FOD work has been extended to three different ceramic matrix composites (CMCs), melt-infiltrated (MI) Sylramic™ SiC/SiC [27], N720/aluminosilicate [28] oxide/oxide, and N720/alumina [29] oxide/oxide CMCs. The most appreciable distinction between the monolithic ceramics and the CMCs

\* Corresponding author. Email address: [sung.choi1@navy.mil](mailto:sung.choi1@navy.mil)

was that the CMCs revealed no catastrophic failure even up to an impact velocity of 400 m/s in which the monolithic counterparts did not survive at all. Recent FOD work also investigated the impact behavior of AS800 and SN282 by using silicon nitride projectiles with varying target thicknesses of 1 mm and 2mm [30].

The current work is to extend the previous work [26,30] to include the effects of target size on FOD by steel ball projectiles. Two different thicknesses of 1 and 2 mm of the flexure targets of AS800 and SN282 were employed with 1.59 mm-diameter hardened steel ball projectiles. The data on  $t=3$ mm previously obtained [25] were also used as a supplementary baseline. Post-impact strength and damage morphology were determined to quantify the severity of related impact damage. Analysis of backside cracking was also made as a function of target thickness and impact velocity based on a simple elastic foundation approach. This paper is considered as a companion to the previous one with ceramic projectiles [30] in terms of target size effect.

## EXPERIMENTAL PROCEDURES

### Target Materials and Test Specimens

Target materials were described elsewhere in the previous work [19-22] and briefly mentioned here again. The materials were two commercial, sintered silicon nitrides, AS800 (fabricated by Honeywell Ceramic Components, Torrance, CA, 1999 vintage) and SN282 (fabricated by Kyocera, Vancouver, WA, 2000 vintage). These two silicon nitrides have been considered as gas-turbine grade in view of their much enhanced toughness and elevated-temperature properties. The SN282 silicon nitride has been recently considered as a candidate for a recuperated ceramic turbo-engine for UAV (Unmanned Air Vehicle) [31]. Figure 1 shows the microstructures of both AS800 and SN282: The AS800 silicon nitride was typified of elongated grain structure. The plates for each material were machined into flexure target specimens measuring 4 mm and 25mm, respectively, in width and length with two different thicknesses of  $t = 1$  and 2 mm. The final finish of target specimens was completed with 600-grit diamond grinding wheel. The basic physical and mechanical properties of both AS800 and SN282 are presented in Table 1.

### Foreign-Object-Damage Testing

Foreign object damage (FOD) testing was conducted using a ballistic impact gun at ambient temperature. Detailed descriptions of the impact apparatus can be found elsewhere [19-22]. Briefly, a hardened steel ball projectile with a

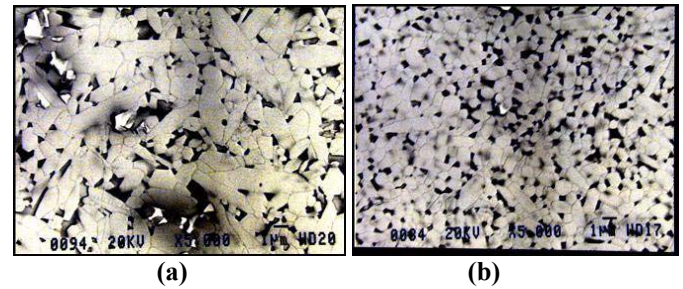


Figure 1. Microstructures of (a) AS800 and (b) SN282 silicon nitrides used in this work.

Table 1. Basic mechanical properties of target and projectile materials at ambient temperature [19,20]

Material		Elastic modulus <sup>1</sup> E (GPa)	Vickers hardness <sup>2</sup> H <sub>v</sub> (GPa)	Flexure strength <sup>3</sup> $\sigma_{fb}$ (MPa)	Fracture toughness <sup>4</sup> (MPa√m)
Targets	AS800 Si <sub>3</sub> N <sub>4</sub>	309	13.6±1.4	775±45	8.1±0.3
	SN282 Si <sub>3</sub> N <sub>4</sub>	304	15.3±0.2	595±64	5.5±0.2
Projectile	Chrome steel (SAE 52100)	200**	8.2±0.2	2200**	-

1. By the impulse excitation technique, ASTM C 1259 [32]; 2. By Vickers microhardness indentation, ASTM C 1327 [33]; 3. By four-point flexure testing, ASTM C 1161 [34]; 4. By single edge precrack beam (SEPB) method, ASTM C 1421 [35]; \*\* From literature data.

diameter of 1.59 mm was inserted into a 300 mm-long gun barrel with an inner diameter of 1.59 mm. Helium-gas in conjunction with relief valves were used to pressurize the reservoir to a specific level, corresponding to a prescribed impact velocity. Upon reaching a specific level of pressure, a solenoid valve was instantaneously opened accelerating the steel ball projectile through the gun barrel to impact a target ceramic specimen. The target specimen was fully supported through a thick steel block (as shown in Fig. 10). Each target specimen was aligned such that the projectile impacted at the center of the target specimen with a normal incidence angle. Impact velocity of projectile was determined using two pairs of laser transmitter and receiver. The range of impact velocity employed in this work was from 20 to 300 m/s. A relatively large number of target specimens, typically 10, were used at each impact velocity for a given material/thickness condition to improve reliability/reproducibility of data while considering a cost issue. In many cases, a relatively small (“a few”) number of target specimens have been used in the literature. Table 1 also includes the basic properties of the silicon nitride ball projectiles.

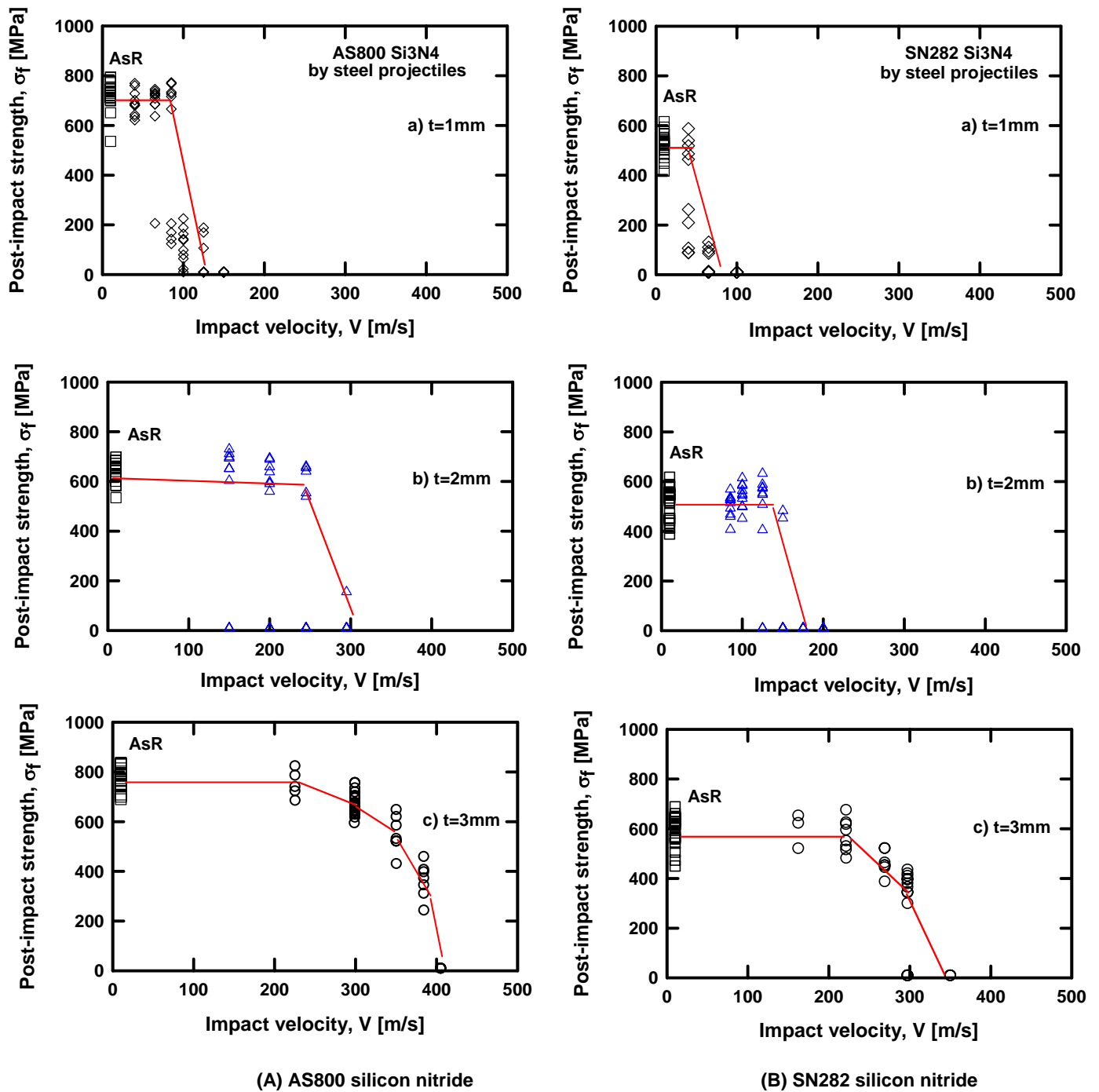


Figure 2. Post-impact flexural strength ( $\sigma_f$ ) as a function of impact velocity (V) for (A) AS800 and (B) SN282 silicon nitrides with different target thicknesses, impacted by 1.59mm-diameter hardened steel ball projectiles at ambient temperature. The data for a target thickness of t=3 mm, determined previously [25], are included for comparison. The “AsR” represents as-received strength with no impact.

### Post-Impact Strength Testing

Strength testing was performed at ambient temperature for the impacted target specimens to assess quantitatively the degree of impact damage, using a four-point flexure fixture with 10-mm inner and 20-mm outer spans. Each impacted target specimen was loaded in the flexure fixture with its impact site being placed to tension within the inner span. An electromechanical test frame (Model 8562, Instron, Canton, MA) was used in displacement control with an actuator speed of 0.5 mm/min. As-received strengths were also determined for each material using a total of 20 specimens for a given target thickness.

## RESULTS AND DISCUSSION

### Post-Impact Strength

The post-impact strength results of AS800 and SN282 with different target thicknesses are presented in Fig. 2, where individual post-impact flexure strength was plotted as a function of impact velocity for each target thickness. The as-received (“AsR”) flexure strength was included for each target thickness. The post-impact strength determined previously with a target thickness of  $t = 3$  mm [25] was also included for comparison. Most of target specimens did fracture in strength testing originating from their impact sites. Exception to this was some of target specimens impacted at lower velocities where resulting impact damage was insignificant or comparable to inherent flaw/defect sizes of the target materials. Post-impact strength decreased with increasing impact, due to increased impact damage. For a given target thickness/impact velocity condition, the impact damage was much greater in SN282 than in AS800. The damage that controlled strength degradation was radial and/or cone cracks emanating from the impact sites, as seen previously [25]. The size of related cracks for a given target thickness/impact velocity was greater in SN282 than in AS800, ascribed to the lower fracture toughness of SN282 (5.5 vs 8.1 MPa√m, see Table 1), thereby resulting in greater strength degradation.

The degradation of post-impact strength of both materials increased with decreasing target thickness, indicative of a target size effect. The thickness effect was attributed to the following facts that: 1) the cracks/damage at impact sites were relatively large as compared to the target thickness with decreasing target size; and 2) the impact event in thinner targets tended to generate additional backside cracks emanating just beneath the impact sites. These dual aspects of cracking/damage contributed greatly to the effect of target size. Impact morphology will be discussed in a later section.

Figure 3 presents the critical impact velocity ( $V_c$ ) as a function of target thickness for the two materials. The critical impact velocity has been defined as a velocity where target specimens were broken catastrophically into two pieces [19-22]. Both of the materials showed an increase in  $V_c$  almost

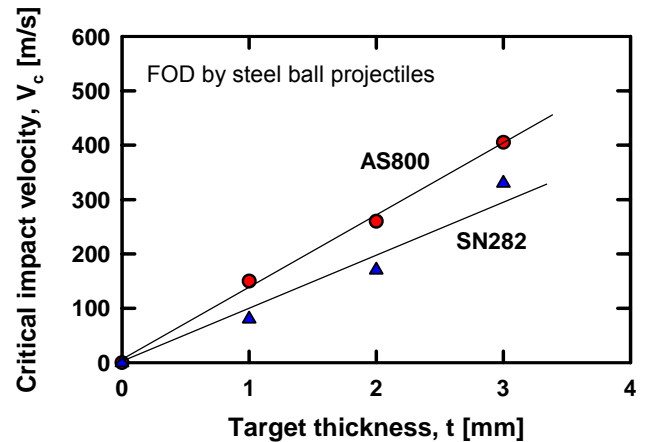


Figure 3. Critical impact velocity ( $V_c$ ) as a function of target specimen thickness ( $t$ ) for AS800 and SN282 silicon nitrides impacted by 1.59mm-diameter hardened steel ball projectiles at ambient temperature. The data for  $t=3$  mm [25] were included for comparison.

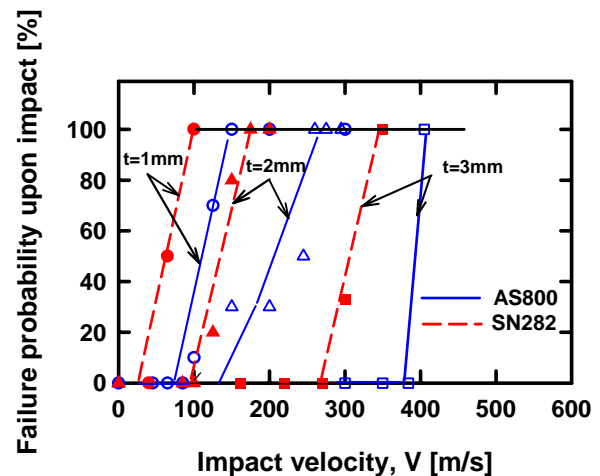


Figure 4. Probability of catastrophic failure upon impact as a function of impact velocity for different target thicknesses for AS800 and SN282 silicon nitrides impacted by 1.59mm-diameter hardened steel ball projectiles at ambient temperature. The data for  $t=3$  mm [25] were included for comparison.

linearly with increasing target thickness. However, AS800 showed greater  $V_c$  for a given target thickness than SN282, due to its greater fracture toughness, as was also observed from the previous work by silicon nitride ball projectiles [30]. The probability of catastrophic failure upon impact is shown in Fig. 4, where failure probability was plotted against impact velocity for three different target thicknesses. The responsiveness of catastrophic failure at the moment of impact was readily discernible from the figure between the two

materials. The  $V_c$  corresponds to the case of a 100% probability of failure upon impact.

The two-parameter, Weibull plots of post-impact strengths for AS800 and SN282 are presented in Fig. 5 for three different target thicknesses. Failure probability ( $\ln[1/(1-F)]$ ) was plotted as a function of strength ( $\ln\sigma$ ). As-received (“AsR”) strengths for  $t=1$  and 2 mm as well as the Weibull plots for  $t=3$  mm previous determined [25] were also included for comparison. The target specimens fractured at  $V_c$ , designated as “CF” in the figure, were plotted with a strength of 10 MPa for a behavioral representation, although they actually yielded a ‘zero’ strength. The Weibull moduli ( $m$ ) of the as-received strengths were  $m=14-21$  and  $9-13$  for AS800 and SN282, respectively, for three different thicknesses. The statistical aspect of FOD damage or strength degradation is clearly seen from the figure. Weibull modulus ( $m$ ) for either AS800 or SN282 rapidly decreased not only with increasing impact velocity but also with decreasing target thickness. At higher impact velocities, Weibull modulus was significantly lower with  $m=1-9$  or the distribution yielded bimodality. The lower  $m$  values are indicative of a wide range of impact damage size. The bimodality was a result of two aspects of fracture such that some specimens broke catastrophically (“CF”) due to significant damage while other specimens retained some finite strength attributed to less but varying degrees of damage. Hence, a transition from unimodality to bimodality took place below the corresponding critical impact velocity. The results of the Weibull distributions also show that post-impact strength was of a stochastic nature. This suggests that the use of only a few samples in FOD tests should be avoided and that a reasonable number of target samples be used to ensure improved reproducibility/reliability of the data.

### **Impact Morphology of Targets and Projectiles**

It has been observed that hardened chrome-steel ball projectiles, upon impacting on AS800 or SN282 targets, were flattened as a result of plastic deformation with their degree of flattening being dependent on impact velocity [19,22,25]. At higher impact velocity ( $>350$  m/s), the hardened steel ball projectiles fractured into several pieces. By contrast, the silicon nitride ball projectiles did not break up to 90 m/s but fractured, shattered or pulverized at impact velocities  $> 90$  m/s [26]. A typical mode of deformation of a steel projectile and its peculiar fracture surface are presented in Fig. 6. The projectile was impacted on a 2mm-thick AS800 target at 250 m/s. Dominant tensile failure of the projectile, which was split into two halves upon impact, is apparent from its fracture surfaces.

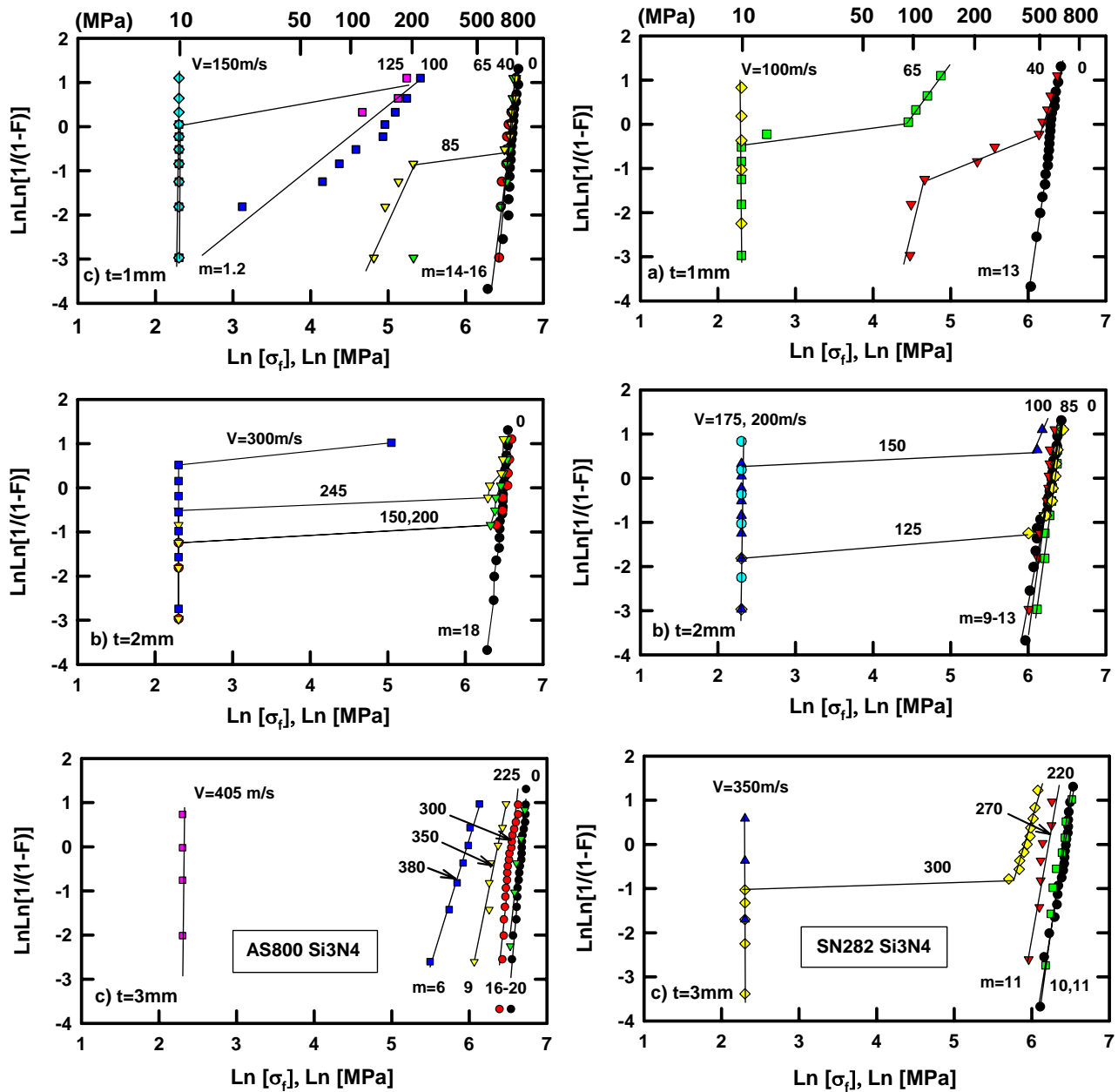
The impact damage generated in target specimens, in general, was typified of plastically deformed impact sites, ring (cone) cracks, and radial cracks with their size/degree

dependent on impact velocity and target thickness. Radial or ring (cone) cracks were primarily responsible for strength degradation. As mentioned in the Post-Impact Strength section, the thin target specimens ( $t=1$  mm) exhibited backside cracking emanating from the point just beneath the impact site. This was due to the localized deflection of targets by impact force associated with deformation of elastic foundation of the steel block support. Typical backside cracks for both AS800 and SN282 are shown in Fig. 7. The severity of backside cracking was greater in SN282 as well as at higher impact velocity. This type of backside cracking was also observed in disk targets (2 mm-thickness and 45 mm-diameter) [21]. The backside cracking is reminiscent of the fracture pattern of disks subjected to biaxial testing. Backside cracking will be discussed and analyzed in more details in a later section.

Examples of fracture surfaces of 2mm-thick targets impacted at 200 m/s are shown in Fig. 8. For SN282, two damage systems of front radial and backside cracks were coexistent; whereas, for AS800, one front radial crack was predominant. Fracture surfaces of the thin targets of  $t=1$ mm were complex in nature because of the presence of both the impact site cracks and the backside cracks. These cracks were not in coplanar in many cases, yielding irregular, rough fracture surfaces.

### **Comparison in FOD Behavior between Steel and Ceramic Ball Projectiles**

Figure 9 shows comparison in post-impact strength between steel ball projectile from this study and silicon nitride ball projectiles determined previously [30]. For a better plotting clarity, data symbols were not included. The difference in post-impact strength between the two different projectile materials becomes more significant with increasing target thickness: The difference was least, intermediate, and greatest, respectively, for  $t=1, 2,$  and  $3$  mm. The size of impact damage (as well as its dual aspect as aforementioned) occurring in thinner targets was comparable to target size, resulting in significant strength degradation, regardless of the type of projectile materials. In thicker targets, the situation was different since the damage created by the ceramic projectiles was much greater than that by the steel projectiles, attributed to much higher Hertzian contact stresses exerted by ceramic projectiles, creating significant strength degradation. The plastically deformed projectiles at the contact point, as shown in Fig. 5, reduced the corresponding contact stresses significantly, resulting in much less cracking and in turn the least strength degradation, as compared with the ceramic counterparts. This again emphasizes the importance of projectile materials with regard to response to impact damage or FOD. This is consistent again with the previous observation [25] that for a given material/impact condition, the hardness of



(a) AS800 silicon nitride

(b) SN282 silicon nitride

Figure 5. Weibull plots of post-impact strengths ( $\sigma_i$ ) of (a) AS800 and (b) SN282 silicon nitrides for different target thicknesses, impacted by 1.59mm-diameter hardened steel ball projectiles at ambient temperature. The data for  $t=3$  mm [25] were included for comparison. F=Failure probability; "CF": Catastrophic failure.

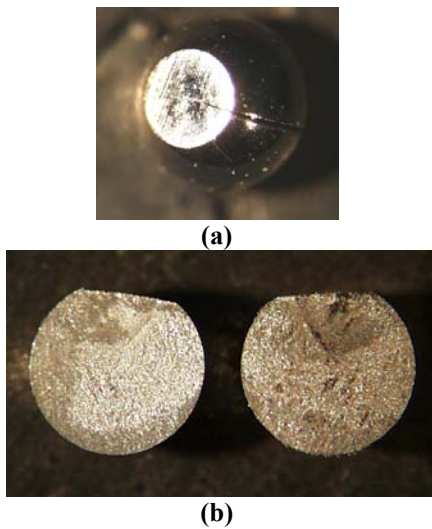


Figure 6. Overall shape (a) and fracture surface (b) of a hardened steel ball projectile split into two upon impact on an AS800 target with  $t=2$  mm at 250 m/s, showing an evidence of tensile failure from the impact site.

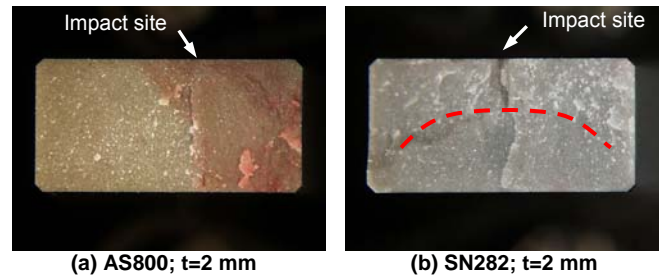


Figure 8. Typical fracture surfaces of target specimens impacted at 200 m/s by 1.59 mm-diameter hardened steel ball projectiles at ambient temperature: (a) AS800; (b) SN282. A backside crack is outlined as a dotted line in (b) SN282.

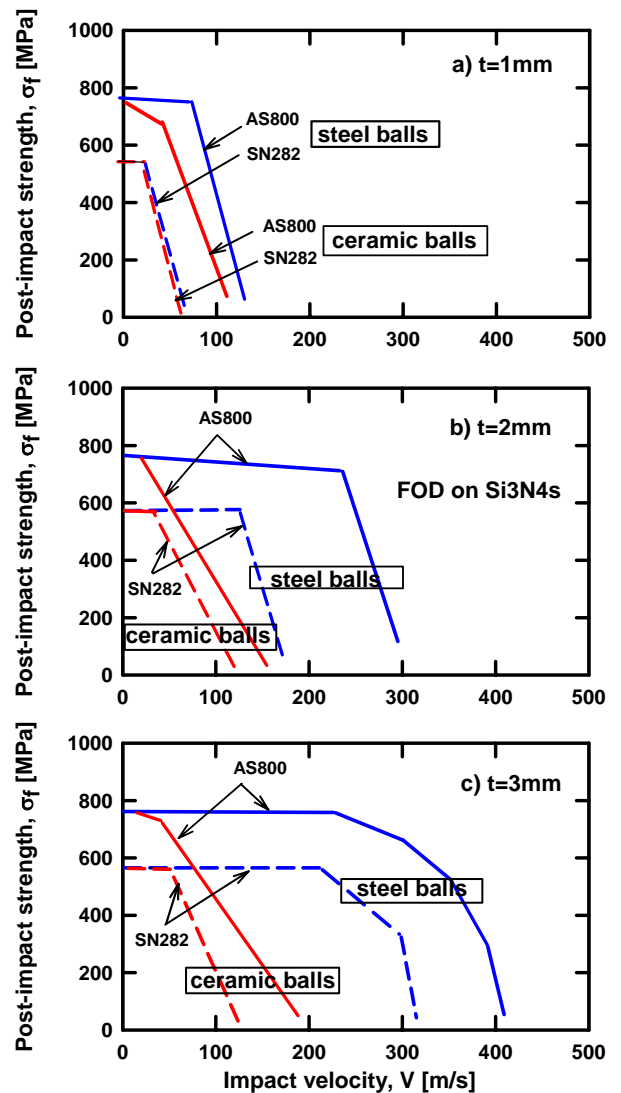


Figure 9. Comparison in post-impact strength between hardened steel ball projectiles (this work) and silicon nitride ball projectiles [30]. The size of projectiles was 1.59 mm diameter for both cases.

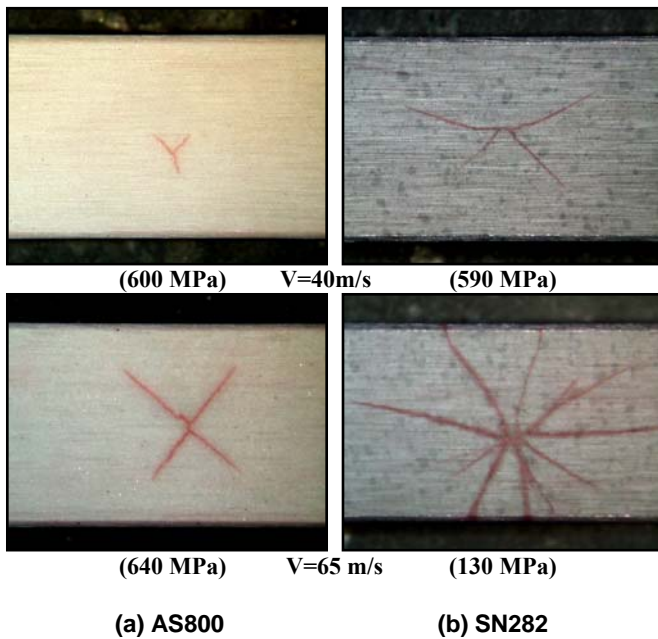


Figure 7. Typical appearances of backside cracking occurring in (a) AS800 and (b) SN282 targets with a thickness of 1 mm, impacted at 40 m/s (above) and 65 m/s (below) by 1.59 mm-diameter hardened steel ball projectiles at ambient temperature. Values of corresponding post-impact strength are also given for each of targets.

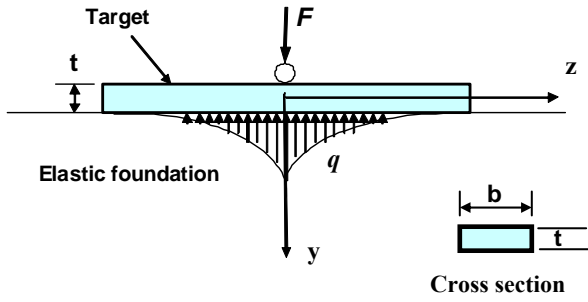


Figure 10. A schematic of elastic foundation considered in the analysis. A target fully supported on elastic foundation is subject to impact force  $F$  by an impacting projectile.

projectiles is a key parameter to affect the most impact damage.

### Backside Cracking and Its Analytical Considerations

As mentioned in the preceding sections, thinner target specimens exhibited a peculiar feature of backside cracking that occurred on the reverse side of targets. Well-defined multiple radial cracks originating from a point just beneath the impact site were typically semi-elliptical in shape. Backside cracking was observed to initiate with an about 50 % probability at  $V=20$  and 40 m/s for SN282 and AS800, respectively; it reached a 100 % probability at 65 m/s for both materials. The size of backside cracks, measured from its center, was around 1-3 mm, depending on impact velocity applied: The higher impact velocity, the greater backside cracks, and *vice versa*.

Although the target specimens were rigidly supported, they were actually supported on an *elastic foundation* of a ‘steel’ block. Any deflection of the elastic foundation by impact force would result in a localized deflection (bending) of the target specimens, which in turn would induce tensile stresses on the reverse side of a target, just beneath the impact site. Backside cracking was analyzed quasi-statically based on a somewhat complex elastic foundation approach [36] to predict the backside cracking velocity. However, it was felt that the approach presented some difficulty in determining certain parameters (particularly the spring constant of related elastic foundation) and that it did not predict the actual pattern of biaxial backside cracking (see the pattern of backside cracking in Fig. 7).

In this study, a rather simplistic, quasi-static approach was made to predict how and when backside cracking occurs as a function of target thickness. As in the general approach, a thin target specimen is assumed to be supported by an elastic foundation as shown in Fig. 10. The maximum tensile stress

( $\sigma_{max}$ ) on the backside of a target due to an impact force ( $F$ ) is governed by linear elasticity and may be generalized as

$$\sigma_{max} = \frac{\alpha F}{bt^2} \quad (1)$$

where  $\alpha$  is an experimentally determined parameter, associated with the elastic foundation as well as the target in conjunction with their configurations, elastic modulus, and Poisson’s ratio, etc. The  $b$  and  $t$  are target width and thickness, respectively. The ‘yield stress’ model [25] can approximate impact force as a function of impact velocity ( $V$ ) for the case of impact of silicon nitride target-versus-hardened steel ball projectile as follows:

$$F = \xi V^q \quad (2)$$

where  $\xi$  and  $q$  are the parameters to be determined for a given combination of target and projectile. Equations (1) and (2) simply yield

$$V = \left[ \left( \frac{b\sigma_{max}}{\alpha\xi} \right) t^2 \right]^{1/q} \quad (3)$$

When  $\sigma_{max}$  reaches the strength of a target material, then backside cracking takes place. In this case,  $V=V_{bc}$  (with  $V_{bc}$  being the backside cracking velocity) and  $\sigma_{max}=\sigma_{fa}$  (with  $\sigma_{fa}$  being the strength of a target material). Therefore, Eq. (3) becomes

$$V_{bc} = \left[ \left( \frac{b\sigma_{fa}}{\alpha\xi} \right) t^2 \right]^{1/q} \quad (4)$$

The critical impact velocity ( $V_c$ ) may be considered to be identical to  $V_{bc}$  for thicker targets of  $t=2$  or 3 mm. Using the SN282 data on  $\sigma_{fa}=595$  MPa (see Table 1),  $b=4$  mm, and  $V_c$  in Fig. 3, together with  $\xi=22.5$  and  $q=1.0$  [5], one can estimate the parameter  $\alpha$  in Eq. (4) to be

$$\alpha = 2.7 \times 10^{-3} \text{ [m]}$$

The units are in Newton for  $F$ , meter/sec for  $V_{bc}$ , and Newton/(meter)<sup>2</sup> for  $\sigma_{fa}$ . Using the experimentally estimated  $\alpha$ ,  $V_{bc}$  can be determined from Eq. (4) for the two target materials as a function of target thickness and the result is presented in Fig. 11. The  $V_{bc}$  data at  $t=1, 2$  mm represent a 50 % probability of backside cracking. As seen from the figure, the prediction is in surprising agreement with the experimental data, despite the lack of in-depth physical insight/elaboration of the model. This implies that the seemingly complex, underlying mechanics behind the backside cracking would be

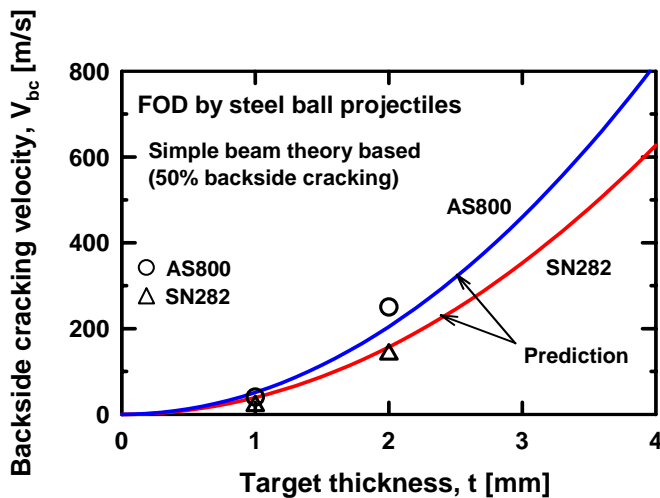


Figure 11. Predicted backside cracking velocity ( $V_{bc}$ ) as a function of target thickness ( $t$ ) for AS800 and SN282 silicon nitrides impacted by 1.59mm-diameter hardened steel ball projectiles at ambient temperature. Experimental data for AS800 and SN282 are included.

rather simple, even operative quasi-statically in an elementary beam or plate theory. The backside cracking for both materials was hardly observed for thicker target specimens with  $t=3$  mm. This would be due to that fact that the backside cracking may coincide with the critical impact velocity so that backside cracking would not be observable since one dominant single crack can control the catastrophic failure of a target.

The occurrence of backside cracking leads to important implications in design of ceramic components if their configurations resemble the type of target support employed in this work. Since the backside damage is much more *significant* in size and degree, overall structural reliability of the components may be controlled by the backside damage than by the front counterpart. Furthermore, the backside damage is *hidden* and NLOS (non-line-of-the-sight) in its configuration. Therefore, an optimum structural design should be exercised to mitigate this type of structurally induced FOD. Also, a pertinent tool such as nondestructive evaluation (NDE) is of necessity for structural assessments.

### FOD Design Considerations

As has been stated, designing aeroengine ceramic components to withstand FOD events is a complex task. Considerations of many factors are needed [17]. A sample of these factors, some of which might be potential tasks of future work, can be listed as follows:

- Effect of primary impact variables such as impact velocity, incidence angle
- Effect of material, geometry, and size of projectiles
- Effect of target material, CMCs or monolithic ceramics, surface condition
- Effect of type, size, and material of target support
- Effect of operating temperature/environment
- Effect of long-term exposure of FOD to service environment
- Effect of protective coatings such as impact barrier coatings, and thermal/environmental barrier coatings (T/EBCs)

It is also noted that FOD is complex both from an analytical standpoint as well as characterizing the phenomena. Appropriate modeling of the phenomena should serve in a feedback loop to experimental techniques, one complementing and improving the other.

### CONCLUSIONS

- 1) Regardless of thickness of target specimens, overall FOD resistance was greater in AS800 than in SN282, attributed to greater fracture toughness of AS800.
- 2) Radial or ring (cone) cracks emanating from the impact sites were observed and primarily responsible for strength degradation.
- 3) Strength degradation and critical impact velocity were significantly dependent on target thickness: The thinner targets yielded greater strength degradation and lower critical impact velocity, and *vice versa*.
- 4) Backside cracking was dominant in the target specimens of a thickness of 1 mm, occurring from a low impact velocity  $\geq 20$  m/s in SN282. A backside cracking analysis based on a simple elastic foundation approach together with a simple beam or plate theory yielded a very reasonable prediction of the backside cracking velocity as a function of target thickness for both AS800 and SN282 silicon nitrides.

### Acknowledgements

This work was supported by the Office of Naval Research and Dr. David Shifler. Some experimental work was performed at NASA Glenn Research Center, Cleveland, OH.

### REFERENCES

1. Wiederhorn, S. M. and Lawn, B. R., 1977, "Strength Degradation of Glass Resulting from Impact with Spheres," J. Am. Ceram. Soc., **60**[9-10], pp. 451-458.

2. Wiederhorn, S. M. and Lawn B. R., 1979, "Strength Degradation of Glass Impact with Sharp Particles: I, Annealed Surfaces," *J. Am. Ceram. Soc.*, **62**[1-2], pp. 66-70.
3. Ritter, J. E., Choi, S. R., Jakus, K., Whalen, P. J., and Rateick, R. G., 1991, "Effect of Microstructure on the Erosion and Impact Damage of Sintered Silicon Nitride," *J. Mater. Sci.*, **26**, pp. 5543-5546.
4. Akimune, Y., Katano, Y., and Matoba, K., 1989, "Spherical-Impact Damage and Strength Degradation in Silicon Nitrides for Automobile Turbocharger Rotors," *J. Am. Ceram. Soc.*, **72**[8], pp. 1422-1428.
5. Knight, C. G., Swain, M. V., and Chaudhri, M. M., 1977, "Impact of Small Steel Spheres on Glass Surfaces," *J. Mater. Sci.*, **12**, pp.1573-1586.
6. Rajendran, A. M. and Kroupa, J. L., 1989, "Impact Design Model for Ceramic Materials," *J. Appl. Phys.*, **66**[8], pp. 3560-3565.
7. Taylor, L. N., Chen, E. P., and Kuzmaul, J. S., 1986 "Microcrack-Induced Damage Accumulation in Brittle Rock under Dynamic Loading," *Comp. Meth. Appl. Mech. Eng.*, **55**, pp. 301-320.
8. Mougnot, R., and Maugis, D., 1985, "Fracture Indentation beneath Flat and Spherical Punches," *J. Mater. Sci.*, **20**, pp. 4354-4376.
9. Evans, A. G., and Wilshaw, T. R., 1977, "Dynamic Solid Particle Damage in Brittle Materials: An Appraisal," *J. Mater. Sci.*, **12**, pp. 97-116.
10. Liaw, B. M., Kobayashi, A. S. and Emery, A. G., 1984, "Theoretical Model of Impact Damage in Structural Ceramics," *J. Am. Ceram. Soc.*, **67**, pp. 544-548.
11. van Roode, M., Jimenez, O., McClain, J., Price, J., Parthasarathy, V., Poormon, K., Ferber, K., and Lin, H.-T., 2002, "Ceramic Gas Turbine Materials Impact Evaluation," ASME Paper No. GT2002-30505.
12. Richerson, D. W. and Johansen, K. M., 1982, "Ceramic Gas Turbine Engine Demonstration Program," Final Report, DARPA/Navy Contract N00024-76-C-5352, Garrett Report 21-4410.
13. Boyd, G. L. and Kreiner, D. M., 1987, "AGT101/ATTAP Ceramic Technology Development," Proceeding of the Twenty-Fifth Automotive Technology Development Contractors' Coordination Meeting, p.101, Dearborn, MI, October 26-29, 1987; SAE, Warrendale, PA.
14. van Roode, M., Brentnall, W. D., Smith, K. O., Edwards, B., McClain, J., and Price, J. R., 1997, "Ceramic Stationary Gas Turbine Development – Fourth Annual Summary," ASME Paper No. 97-GT-317.
15. Akimune, T, Akiba, T., and Ogasawara, T., 1995, "Damage Behavior of Silicon Nitride for Automotive Gas Turbine Use When Impacted by Several Types of Spherical Particles," *J. Mater. Sci.*, **30**, pp. 1000-1004.
16. Yoshida, H, Kano, S., Hasegawa, Y., Shimamori, T., and Yoshida, M., 1996, "Particle Impact Phenomena of Silicon Nitride Ceramic," *Philo. Magazine A*, **74**[5], pp. 1287-1297.
17. Peralta, A. D. and Yoshida, H., 2003, Ceramic Gas Turbine Component Development and Characterization, van Roode, M, Ferber, M. K., and Richerson, D. W., eds., Vol. 2, pp. 665-692, ASME, New York, NY.
18. Deshpande, V.S. and Evans, E.G., 2008, "Inelastic Deformation and Energy Dissipation in Ceramics: A Mechanism-Based Constitutive Model," *J. Mech. Phys. Solids*, **56**, pp. 3077-3100.
19. Choi, S. R., Pereira, J. M., Janosik, L. A., and Bhatt, R. T., 2002, "Foreign Object Damage of Two Gas-Turbine Grade Silicon Nitrides at Ambient Temperature," *Ceram. Eng. Sci. Proc.*, **23**[3], pp. 193-202.
20. Choi, S. R., Pereira, J. M., Janosik, L. A., and Bhatt, R. T., 2004, "Foreign Object Damage in Flexure Bars of Two Gas-Turbine Grade Silicon Nitrides," *Mater. Sci. Eng. A* **379**, pp. 411-419.
21. Choi, S. R., Pereira, J. M., Janosik, L. A., and Bhatt, R. T., 2003, "Foreign Object Damage of Two Gas-Turbine Grade Silicon Nitrides in a Thin Disk Configuration," ASME Paper No. GT2003-38544.
22. Choi, S. R., Pereira, J. M., Janosik, L. A., and Bhatt, R. T., 2004, "Foreign Object Damage in Disks of Gas-Turbine-Grade Silicon Nitrides by Steel Ball Projectiles at Ambient Temperature," *J. Mater. Sci.*, **39**, pp. 6173-6182.
23. Choi, S. R., Racz, Z., Bhatt, R. T., Brewer, N. N., and Gyekenyesi, J. P., 2005, "Effect of Projectile Materials on Foreign Object Damage of a Gas-Turbine Grade Silicon Nitride," ASME Paper No. GT2005-68866.
24. Choi, S. R., et al., 2006 "Foreign Object Damage in a Gas-Turbine Grade Silicon Nitride by Spherical Projectiles of Various Materials," NASA TM-2006-214330, NASA Glenn Research Center, Cleveland, OH.
25. Choi, S. R., 2008, "Foreign Object Damage Behavior in a Silicon Nitride Ceramic by Spherical Projectiles of Steels and Brass," *Mater. Sci. Eng. A* **497**, pp. 160-167.
26. Choi, S. R., 2009, "Foreign Object Damage in Gas-Turbine Grade Silicon Nitrides by Silicon Nitride Ball Projectiles," ASME Paper No. GT2009-59031.
27. Choi, S. R., 2008, "Foreign Object Damage Phenomenon by Steel Ball Projectiles in a SiC/SiC Ceramic Matrix Composite at Ambient and Elevated

- Temperatures,” J. Am. Ceram. Soc. **91**[9], pp. 2963-2968 (2008).
28. Choi, S. R., Alexander, D. J., and Kowalik, R. W., 2008, “Foreign Object Damage in an Oxide/Oxide Composite at Ambient Temperature,” ASME Paper No. GT2008-50505; also in 2009, J. Eng. Gas Turbines & Power, **131**, pp. 021301-1\_6.
  29. Faucett, D. C., Alexander, D. J., and Choi, S. R., 2010, “Static-Contact and Foreign-Object-Object Damages in an Oxide/Oxide (N720/Alumina) Ceramic Matrix Composite: Comparison with N720/Aluminosilicate,” *Processing & Properties of Advanced Ceramics & Composites*, Ceramic Transactions, **220**, pp. 221-242.
  30. Choi, S.R. and Rácz, Z., 2010, “Target Size Effects on Foreign Object Damage in Gas-Turbine Grade Silicon Nitrides by Ceramic Ball Projectiles,” ASME Paper No. GT2010-23574.
  31. Vick, M. J., Heyes, A., and Pullen, K., 2009, “Design Overview of A Three-Kilowatt Recuperated Ceramic Turboshaft Engine,” ASME Paper No. GT2009-60297.
  32. ASTM C 1259, Annual Book of ASTM Standards, Vol. 15.01, ASTM, West Conshohocken, PA (2008).
  33. ASTM C 1327, *ibid*, ASTM, West Conshohocken, PA (2008).
  34. ASTM C 1161, *ibid*, ASTM, West Conshohocken, PA (2008).
  35. ASTM C 1421, *ibid*, ASTM, West Conshohocken, PA (2008).
  36. Boresi, A. P., Sidebottom, O. M., Seely, F. B., and Smith, J. O., *Advanced Mechanics of Materials* (3<sup>rd</sup> Edition), pp. 369-377, John Wiley & Sons, NY (1978); also see any text books on advanced mechanics.